# Exploiting dynamical symmetry in coupled nonlinear elements for efficient frequency down-conversion

Patrick Longhini,[1,*] Antonio Palacios,[2,†] Visarath In,[1,‡] Joseph D. Neff,[1] Andy Kho,[1] and Adi Bulsara[1]
[1]*Space and Naval Warfare Systems Center, Code 2373, 53560 Hull Street, San Diego, California 92152-5001, USA*
[2]*Nonlinear Dynamical Systems Group, Department of Mathematics, San Diego State University, San Diego, California 92182, USA*
(Received 22 May 2007; published 1 August 2007)

The rich dynamical behavior stemming from unidirectional coupling in a single array of overdamped nonlinear elements has, recently, been extensively studied. By adjusting control parameters, one obtains regimes of oscillations with a frequency that scales in a characteristic way with the control parameter. With an external time-sinusoidal driving signal, a richness of synchronized (to the drive frequency or its subharmonics depending on the control parameter) dynamical behavior ensues. Including $M \geqslant 2$ arrays with a suitably chosen cross coupling has also been shown to lead to multifrequency patterns in the emergent dynamics. Here, we consider this arrangement and demonstrate that, under the appropriate conditions, the oscillation frequency of each successive array decreases by a rational factor with increasing $M$. This frequency down-conversion, obtainable without a heterodyning signal, affords the promise of very efficient signal processing in a variety of applications wherein, currently, the frequency down-conversion stage typically involves multistep processes with complicated and (often) noisy circuitry.

DOI: 10.1103/PhysRevE.76.026201 PACS number(s): 05.45.Xt

## I. INTRODUCTION

Nonlinear physical systems are known to show very rich spatiotemporal behavior as has been demonstrated in areas as diverse as biology [1] and fluid mechanics [2]. In particular, multifrequency spatiotemporal behavior has been reported in systems of coupled bistable elements [3]. In our previous work [4–6], we described the emergence of oscillations in a unidirectionally coupled ring of $N$ overdamped bistable elements; this novel behavior is already being exploited in a new class electric and magnetic field detectors wherein a ring of unidirectionally coupled nonlinear components comprises the "active" element of the detector. In addition, we have shown the implications of symmetry together with the array dynamics in the generation of multifrequency oscillations in coupled *arrays* of (excitable) nonlinear elements [7]; one finds, in particular, that frequency upconversion by a factor of $N$ is possible, with bidirectional (in contrast to the current work) interarray coupling.

Frequency downconversion, on the other hand, is more complicated to generate via coupled nonlinear array dynamics; it is, however, a critical step in many modern signal processing applications wherein a high-frequency signal must be down-converted before it can be applied to an analog-to-digital converter (ADC). Various means (most involving some form of heterodyning with a reference signal) are employed to this end, but they are, sometimes, inefficient and often the procedure can raise the noise floor of the device through the heterodyne signal generator.

In this work we show how a high-frequency signal can be down-converted by passing it through a cascade of arrays of unidirectionally coupled overdamped bistable elements. The coupling scheme as well as the choice of element dynamics is very different from our earlier work [7]; accordingly, the mechanism of down-conversion is also significantly different. As an example, we find that the frequency down-conversion can be by a factor of 1/2, 1/5, or 1/11 for two coupled arrays of three elements ($N=3, M=2$). A generalization to larger $M$ is also provided. While our work lays the foundation for very efficient down-conversion for a variety of practical applications, we focus the current paper only on a first reporting of the theoretical (including numerical) results. We use analysis tools that emphasize the symmetry of the networks to help us better understand the organization and stability properties of the ensuing behavior while providing the means for determining both invariance and changes in the system without going deep into the analysis of its dynamics. We note that the robustness of a given network guarantees that certain patterns of oscillation persist regardless of the internal dynamics of each individual nonlinear element.

## II. NETWORK CONFIGURATIONS AND SYMMETRIES

We define a *cell* as an individual element, typically represented via the evolution of a state variable, $\dot{x}=f(x,\alpha)$, with the overdot denoting a time derivative and $\alpha \in \mathbb{R}^p$ a vector of cell parameters. Further, $f:\mathbb{R}^n \times \mathbb{R}^p \mapsto \mathbb{R}$ is a smooth function. There are inherent properties of the network dynamics that may be restricted by symmetry, including *local* (dictated by individual cell dynamics) and *global* (predicated by the coupling) symmetries [8]. The dynamics of an individual cell in an array are represented by $\dot{x}_i=f(x_i,\alpha)+\Sigma_{j\to i}\lambda_{ij}h(x_i,x_j)$, where $x_i=(x_{i1},\ldots,x_{ik}) \in \mathbb{R}^k$ denote the state variables of cell $i$ and the function $h$ defines the coupling (having strength $\lambda_{ij}$) between cells $i$ and $j$.

We start with a special case of the more general setup depicted in Fig. 1, a network of two coupled arrays with dynamics described by

*longhini@spawar.navy.mil
†palacios@euler.sdsu.edu
‡visarath@spawar.navy.mil

 ©2007 The American Physical Society

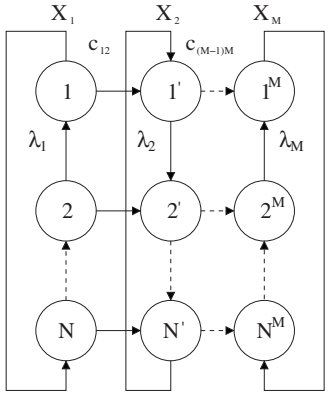


FIG. 1. Generalized network configuration of $M$ arrays of coupled cell units. Each array contains $N$ elements.

$$\dot{x}_i = f(x_i, \alpha) + \sum_{j \to i} \lambda_{ij} h(x_i, x_j),$$

$$\dot{y}_i = f(y_i, \alpha) + \sum_{j \to i} \lambda_{ij} h(y_i, y_j) + c_{ij} k(y_i, x_j), \tag{1}$$

where $y_i = (y_{i1}, \ldots, y_{ik}) \in \mathbb{R}^k$ denote the state variables of cell $i$ in the second array and $k$ is an interarray coupling function, $c_{ij}$ being the corresponding coupling strength. Notice the unidirectional coupling in each array and also between adjacent cells in the two arrays. The opposite directions of the intra-array couplings should also be noted. The unidirectional interarray coupling yields a network with global symmetry described by the direct product group $Z_N \times Z_N$, in which $Z_N$ is the group of cyclic permutations of $N$ objects. Each element of the direct product group permutes, simultaneously, each element of the corresponding arrays. For the moment, there is no externally applied signal.

To study the patterns of behavior for the $M=2$ case of the network in Fig. 1, we use $X_1(t) \equiv X(t) = (x_1(t), \ldots, x_N(t))$ to represent the state of one array and $X_2(t) \equiv Y(t) = (y_1(t), \ldots, y_N(t))$ to denote the state of the second array. Thus, at any given time $t$, a spatiotemporal pattern generated by the network can be described by $P(t) = (X(t), Y(t))$. To begin the analysis, let us assume that both arrays exhibit a traveling-wave (TW) pattern with period $T$. That is, the wave forms produced by each array are identical, but out of phase by a constant time lag $\phi = T/N$. We also make a second assumption that the $X_2$ array oscillates at $m$ times the period of the $X_1$ array, where $m$ is a nonzero integer. Thus, $P(t)$ has the form

$$P(t) = (x(t), x(t + (N-1)\phi), \ldots, x(t+\phi), y(t), y(t + m\phi), \ldots, y(t + (N-1)m\phi)), \tag{2}$$

where the $X_1$ array exhibits a TW in the opposite direction of the $X_2$ array, a direct result of the opposite orientation of their coupling schemes. For simplicity, we further assume that $N=3$ and that the units are coupled as is shown in Fig. 1. From Eqs. (2), a solution to this network has the form

$$P(t) = \left(x(t), x\left(t + \frac{2T}{3}\right), x\left(t + \frac{T}{3}\right), y(t), y\left(t + \frac{mT}{3}\right), y\left(t + \frac{2mT}{3}\right)\right). \tag{3}$$

Now assume that $P(t)$ has spatiotemporal symmetry described by the cyclic group $\Gamma \equiv Z_3 \times Z_3$ and by the group $S^1$ of temporal shifts. Together, $\Gamma \equiv Z_3 \times Z_3 \times S^1$ acts on $P(t)$ as follows. First, $\Gamma$ acts as a permutation: $\Gamma: (1,2,3,1',2',3') \mapsto (3,1,2,3',1',2')$, so that

$$\Gamma P(t) = \left(x\left(t + \frac{T}{3}\right), x(t), x\left(t + \frac{2T}{3}\right), y\left(t + \frac{2mT}{3}\right), y(t), y\left(t + \frac{mT}{3}\right)\right). \tag{4}$$

Then $S_1$ shifts time by $mT/3$ so that

$$\left(\Gamma, \frac{mT}{3}\right) P(t) = \left(x\left(t + \frac{m+1}{3}T\right), x\left(t + \frac{m}{3}T\right), x\left(t + \frac{m+2}{3}T\right), y(t + mT), y\left(t + \frac{m}{3}T\right), y\left(t + \frac{2m}{3}T\right)\right). \tag{5}$$

Since the cells are assumed to be identical, it follows that $\Gamma \equiv Z_3 \times Z_3 \times S^1$ is a spatiotemporal symmetry of the network provided that $X(t) = X\left(t + \frac{m+1}{3}T\right)$ and $Y(t) = Y(t + mT)$. But $X_1$ is $T$ periodic, which implies that $m = 3k-1$, where $k$ is a nonzero integer. As $k$ increases (starting at 1) we obtain the following values for $m$: 2,5,8,11,14,17,20,23,…. When $m=2$, for instance, the $X_2$ array oscillates at $1/2$ the frequency of the $X_1$ array. Likewise, $m=5$ suggests that the $X_2$ array oscillates at $1/5$ the frequency of the $X_1$ array. The case when $m=8$ should be excluded, however, since $m = 8 = 2^2 \times 2$.

As $N$ increases, similar frequency down-conversion ratios emerge. A bifurcation analysis shows that the regions of existence of these frequency ratios form a well-defined partition, in parameter space $(\lambda_2, c_{xy})$, which is reminiscent of Arnold's tongue structures. In general we find (noting that $N$ is odd) $\omega_{X_1}/\omega_{X_2} = N-1, 2N-1, \ldots, Nk-1$.

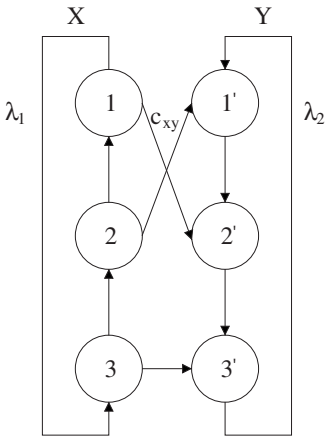


FIG. 2. Network of two coupled arrays similar to that of Fig. 1, except for the cross-coupling scheme. This network also affords various frequency down-conversion ratios.

One would expect that analogous behavior is obtained when the cross-coupling topology is altered, as shown in Fig. 2, for example; the global symmetries of this network are now defined by

$$\Gamma(3,2,1,1',2',3') \mapsto (2,1,3,2',3',1').$$

Repeating a similar analysis (not shown for brevity) leads us to conclude that this latest group of symmetries would force the $Y$ array to oscillate at $(1,4,7,\ldots,3k-2)$ times the period of the $X$ array in addition to the 1/2- and 1/5-frequency relations of the previous network. Again a well-defined partition associated with the various down-conversion ratios are found, in the parameter space $(\lambda_2, c_{xy})$, for larger arrays.

## III. SIMULATIONS

To verify the existence of these oscillations, we define the individual dynamics of each cell to be that of a prototypical bistable system, an overdamped Duffing oscillator with internal dynamics given by $f(x)=ax-bx^3$ and the (unidirectional) intra-array coupling functions by $h(x_i,x_{i+1})=x_i-x_{i+1}$ and $h(y_i,y_{i-1})=y_i-y_{i-1}$, respectively. The interarray connections are unidirectional as shown in Fig. 1; hence, the $X_1$-array dynamics has no dependence on the $X_2$-array dynamics. Then, the network dynamics are represented by the system

$$\tau\dot{x}_i = ax_i - bx_i^3 + \lambda_1(x_i - x_{i+1}),$$

$$\tau\dot{y}_i = ay_i - by_i^3 + \lambda_2(y_i - y_{i-1}) + c_{xy}x_i, \tag{6}$$

where $i=1,\ldots,N$ mod $N$, $a$ and $b$ are positive constants that describe the dynamics of the individual cells, and $\lambda_1$ and $\lambda_2$ define the intra-array coupling strengths for the $X_1$ and $X_2$ arrays, respectively, with $c_{xy}$ the interarray coupling coefficient. $\tau$ is a system time constant.

First assume that there is no cross coupling—i.e., $c_{xy}=0$. Then [6], $\lambda_{1c}=a/2$ is the critical coupling strength beyond which the $X_1$ elements oscillate. Accordingly, if the coupling strength of the $X_2$ array is below the critical coupling strength, i.e., $\lambda_2<\lambda_c$, and the coupling strength of the $X_1$ array is above, $\lambda_1>\lambda_c$, then we would obtain the pattern shown in the left panel of Fig. 3 for the $X_1$ elements, but the $X_2$ array would be quiescent.

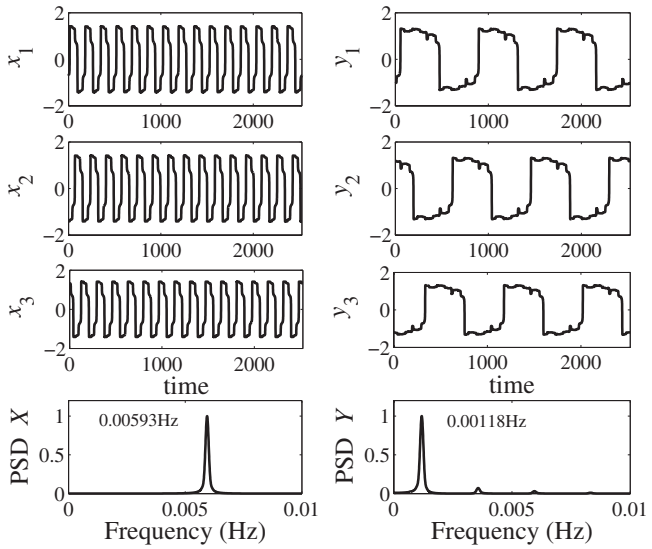


FIG. 3. Numerical simulations showing the frequency down-conversion effect. The bottom panels depict the corresponding power spectra density (PSD) where it can be checked that each element in the $X_2$ array oscillates at 1/5 the frequency of each element in the $X_1$ array $(0.001186\ \text{Hz} \approx \frac{1}{5}0.00593\ \text{Hz})$. Parameters are $c_{xy}=0.14$, $\lambda_1=0.51$, $\lambda_2=0.3$, $a=1$, $b=1$, and $\tau=1$.

Increasing the cross-coupling strength $c_{xy}>0$ induces the $X_2$ array to oscillate (above a critical value of $c_{xy}$) with frequency $\omega_{X_2}=\omega_{X_1}/5$; this is shown in the bottom right panel of Fig. 3. Increasing further the cross coupling $c_{xy}$ causes the $X_2$ array to oscillate at 1/2 the frequency of the $X_1$ array. Additional frequency down-conversion ratios 1/2, 1/5, and $1/(3k-1)$, where $k=1,2,3,\ldots$, are also observed as the cross coupling $c_{xy}$ increases further.

## IV. CASE OF A TIME-PERIODIC INPUT SIGNAL

So far, we have considered emergent oscillations, and the frequency down-conversion resulting from the intra-array coupling depicted in Fig. 1, in the absence of an external signal. The oscillations emerge when the control parameters (the coupling coefficients) push the system through a critical point, it being assumed, always, that all the elements had random initial conditions (as in any reasonable physical system). As in our previous work (for the $M=1$ case) [5,6], the emergent oscillations in each cell of the array are nonsinusoidal and have a well-defined phase difference (between cells), and the frequency shows a characteristic scaling behavior with the control parameter(s), in this case the coupling coefficients.

The above considerations allow us to transition, smoothly, to the discussion of the down-conversion effect when an

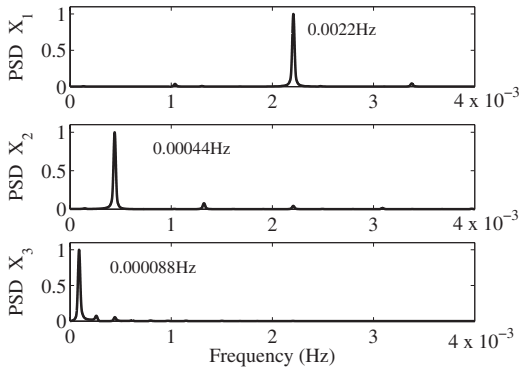


FIG. 4. Frequency down-conversion of an ac signal to 1/75th of its original frequency via a network cascade of $M=3$ coupled arrays. The $X_1$ array receives the input signal with frequency $f=0.0066$ Hz; it then generates a TW pattern of oscillations with frequency $f/3=0.0022$ Hz. The $X_2$ array, in turn, down-converts the frequency of the TW pattern by a factor of 5. A third array $X_3$ lowers even more the frequency of the TW pattern to $f/75=0.000088$ Hz. Parameters are $N=3$, $M=3$, $(\lambda_1,\lambda_2,\lambda_3,c_{x_{12}},c_{x_{23}})=(0.51,0.3,0.3,0.14,0.14)$, $\omega=2\pi f=0.04188$, and $\varepsilon=0.01$.

external sinusoidal signal $\varepsilon \sin \omega t$ is applied to the $X_1$ array. The network equations (6) are then augmented by the term $\varepsilon \sin \omega t$ on the right-hand side (rhs) of the $x_i$ dynamics. Intuitively, one would believe that, because of the unidirectional interarray coupling, the above considerations (specifically, the frequency down-conversion ratios for $\omega_{X_2}/\omega_{X_1}$) still hold true; once the response of the $X$ array is known, the frequency can be down-converted through a suitable choice of the coupling parameters $\lambda_2$ and $c_{xy}$. Numerical simulations indicate that this is, indeed, the case although additional frequency entrainment between the external signal and the oscillations of the $X_1$ array must be taken into consideration. The response of the $X_1$ array to the external signal was quantified in [6,9] for different (soft-potential) coupled systems. We have shown (Fig. 4 in [6]) that, depending on the parameters $\varepsilon$ and $\lambda_1$, the frequency $\omega_{X_1}$ of each element in the $X_1$ array can be entrained to $\omega/n$ with $n$ a positive integer. Then, given the frequency $\omega_{X_1}$, the response of the $X_2$ array is activated by setting $c_{xy}>0$ and the frequency down-conversion ratios already obtained above are now applied to, in essence, the external frequency $\omega$. As an example, we consider the case of the $X_1$ array entrained to the frequency $\omega_{X_1}=\omega/3$ (corresponding to region II in Fig. 4 of [6]). When the cross coupling is activated to $c_{xy}=0.14$ we observe the 1/5-frequency down-conversion from the $X_1$ array and the effective frequency of the $X_2$ array is (Fig. 4) 1/15 the frequency of the applied periodic signal.

We would expect that extending our results to a cascade of coupled networks ($M>2$), with each array down-converting the frequency of the preceding array via the rules already described above, should be readily possible. We find, in fact, that a network of multiple arrays can achieve a lowering of frequencies in each successive array. A mathematical representation of the network is given by the following system of ordinary differential equations (ODEs):

$$\begin{aligned}
\dot{x}_{1i} &= a x_{1i} - b x_{1i}^3 + \lambda_1 (x_{1i} - x_{1(i+1)}) + \varepsilon \sin(\omega t), \\
\dot{x}_{2i} &= a x_{2i} - b x_{2i}^3 + \lambda_2 (x_{2i} - x_{2(i-1)}) + c_{12} x_{1i}, \\
&\vdots \quad = \quad \vdots \\
\dot{x}_{Mi} &= a x_{Mi} - b x_{Mi}^3 + \lambda_m (x_{Mi} - x_{M(i-(-1)^M)}) + c_{(M-1)M} x_{(M-1)i},
\end{aligned} \tag{7}$$

where $i=1,\ldots,N \bmod N$, $\lambda_j$ corresponds to the coupling of array $j$, for $j=1,\ldots,M$, $c_{x_{jl}}$ denotes the coupling from array $j$ to array $l$, and $M$ is the total number of arrays coupled together. Notice that all the arrays are coupled unidirectionally from one to another and the elements within each individual array are also unidirectionally coupled, but the direction of coupling alternates from one array to the next—i.e., from clockwise to counterclockwise and so on. This pattern of coupling has been chosen so that the bifurcations that lead to the multifrequency patterns are still present in the network.

As an example, let $N=3$, $M=3$, so that oscillations in the $X_1$ array occur only when $\lambda_1>a/2=0.5$. The existence of multifrequency patterns in each successive array ($j>1$) requires $\lambda_j<0.5$. Thus, by setting the intra-array coupling strengths to $(\lambda_1,\lambda_2,\lambda_3)=(0.51,0.3,0.3)$ and the cross coupling to $(c_{x_{12}},c_{x_{23}})=(0.14,0.14)$ we achieve a down-converting of frequency from the $X_1$ array to the $X_2$ array and again from the $X_2$ array to the $X_3$ array. We reiterate that when the cross coupling $(c_{12},c_{23})$ is turned off, or set below the critical values, the elements in the $X_2$ and $X_3$ arrays are quiescent. So we can conclude that the oscillations emerge directly from the cross-coupling terms. As seen in Fig. 4, our choice of parameters leads to $\omega_{X_1}/\omega_{X_2}=5=\omega_{X_2}/\omega_{X_3}$, so that a signal of frequency $\omega$ which causes the $X_1$-array elements to entrain at frequency $\omega_{X_1}=\omega/3$ is, finally, down-converted to $\omega_{X_3}=\omega/75$ at the output of the $X_3$ array.

## V. BIFURCATION ANALYSIS

In order to quantify the actual mechanisms for the existence and stability of the various frequency down-conversion patterns, we now carry out a bifurcation analysis, employing the numerical computation package AUTO [10]. We consider, for clarity, the case $N=3$, $M=2$, although the analysis can be readily extended to larger networks as well as networks with different interarray coupling patterns. Holding $\lambda_1$ fixed past the critical value $\lambda_{1c}(=a/2)$ that is required for the $X_1$ array to oscillate, we obtain the two-parameter bifurcation diagram (solid curves) shown in Fig. 5. Five distinct regimes are depicted in that figure. (I) Supercritical regime: both arrays oscillate in a TW pattern. But as $\lambda_2$ increases, the frequency of the $X_2$ array ($\omega_{X_2}$) locks, during certain intervals of $\lambda_2$, onto various submultiples of the frequency of the $X_1$ array ($\omega_{X_1}$)—i.e., $\omega_{X_2}=\omega_{X_1}/m$, where $m=2,5,11,17,23$. Figure 6 illustrates the actual intervals of frequency locking. (I′) Two in-phase regime: wherein two oscillatory units (of each array) share the same phase and same amplitude, but the third

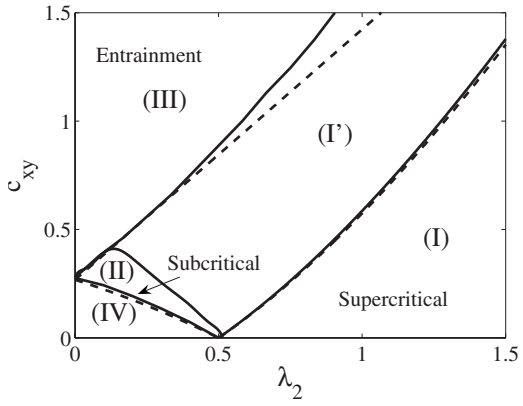


FIG. 5. Regimes of frequency relations (see text) between the two coupled arrays $X_1$ and $X_2$ of the network of overdamped Duffing elements shown in Fig. 1. Solid curves are obtained numerically via AUTO; dashed curves are computed analytically.

one is out of phase by $\pi$. This pattern of oscillation has been predicted in related work [11]. (II) Subcritical regime: frequency down-conversion by $1/2, 1/5, \ldots, 1/(3k-1)$ (where $k=1,2,3,\ldots$) of the frequency of the $X_1$ array. By setting the $X_2$-array coupling below the critical coupling ($\lambda_2=0.4<\lambda_c$) and varying the frequency of the $X_1$ array, we find that these frequency down-conversion rates form a well-defined partition of the $c_{xy}$-frequency ($X_1$) plane, as is shown in Fig. 7. The size of each partition seems to get smaller as the frequency down-conversion rate increases, in a manner that is reminiscent of the well-known Arnold's tongues. (III) Entrainment regime: frequency locking of each individual $y_i$ element to its corresponding $x_i$ element. (IV) No oscillations regime: oscillations do not exist and the system settles, instead, to a steady state. Note that the boundary curve that separates region II from I′ is not an actual bifurcation curve. Moving from region II to I′ does not change the characteristics (frequency and amplitude) of the oscillations; rather, only the phase of the TW pattern found in region II changes, with two of the units entraining their phases while the third unit oscillates out of phase by $\pi$. We show this boundary curve for completeness purposes, however.

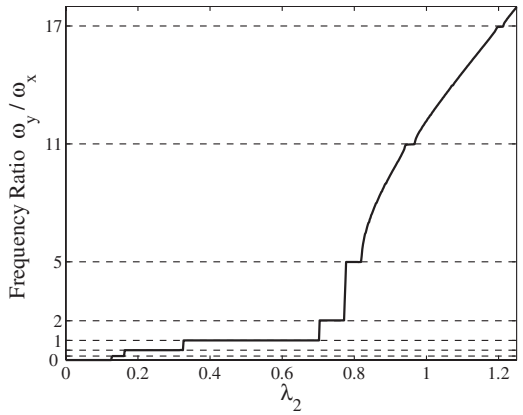


FIG. 6. Frequency relation between the $X_1$ and $X_2$ arrays for the network configuration of Fig. 1 as a function of coupling strength $\lambda_2$.

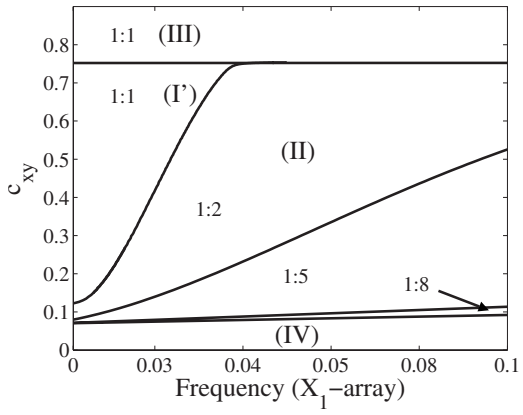


FIG. 7. Partition of frequency down-conversion rates, in the $c_{xy}$-frequency ($X_1$) plane, between the $X_1$ and $X_2$ arrays. Coupling strength of the $X_2$ array is set below the critical coupling $\lambda_2=0.4$.

For larger values of the coupling strength in the $X_2$ array—i.e., past the critical coupling—the partition of frequency down-conversion rates changes as can be observed in Fig. 8.

Next we compute an analytical expression for the critical cross coupling $c_{xy}$ curves shown in Fig. 5 (solid curves). From numerical simulations we know that, at the onset of the oscillations in the $X_2$ array, only one element ($y_1$, say) changes while the others remain in an upper or lower state $y_{2m}$ (i.e., the elements evolve in sequence); in previous work [6], $y_{2m}$ was found to be ($\tau=1$ for simplicity)

$$y_{2m} = \sqrt{\frac{a+2\lambda_2}{b}} + \frac{c_{xy}x_{1m}}{2(a+2\lambda_2)}. \tag{8}$$

The $X_1$ array exhibits similar behavior except that the amplitude of the applied ac signal replaces the cross-coupling term:

$$x_{1m} = \sqrt{\frac{a+2\lambda_1}{b}} + \frac{\varepsilon}{2(a+2\lambda_1)}. \tag{9}$$

Using Eqs. (8) and (9), the evolution of $y_1$ [from Eq. (6)] is given by

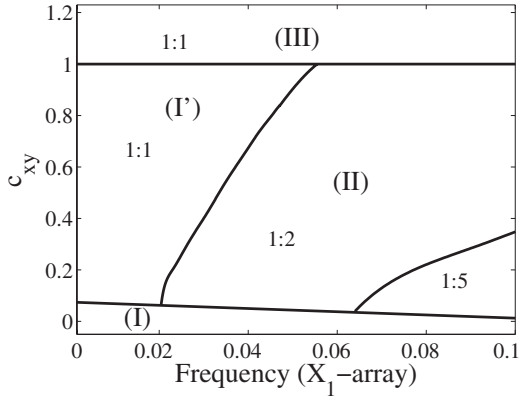


FIG. 8. Partition of frequency down-conversion rates similar to those of Fig. 7 except that the coupling strength is now $\lambda_2=0.6$, which is above the critical coupling of the $X_2$ array.

$$y_1 = (a + \lambda_2)y_1 - by_1^3 + \lambda_2(y_{2m}) + c_{xy}x_{1m}. \tag{10}$$

Then, following the techniques developed in [6], we arrive at the following expression for the critical amplitude:

$$c_{xy}^c x_{1m} = (F_0 - \lambda_2 y_{2m}) + k_1\{\omega^2[(c_{xy}^c x_{1m})^2 - (F_0 - \lambda^2 y_{2m})^2]\}^{1/3}, \tag{11}$$

where $F_0 = \sqrt{4(a+\lambda_2)^3/(27b)}$, $\omega$ is the frequency of the applied ac signal, and $k_1$ is a fitting parameter. The three roots for $c_{xy}^c$ in Eq. (11) are

$$c_{xy}^c = \frac{F_0 - \lambda_2 e}{(1 + \lambda_2 f)x_{1m}},$$

$$c_{xy}^c = \frac{1}{x_{1m}}\left[\frac{2(F_0 - \lambda_2 e)(1 + \lambda_2 f) + k_1^3(1 - \lambda_2 f)\omega^2}{2(1 + \lambda_2 f)^2} \pm \frac{\sqrt{k_1^3\omega^2[8(F_0 - \lambda_2 e)(1 + \lambda_2 f) - k_1^3\omega^2(1 - \lambda_2 f)]}}{2(1 + \lambda_2 f)^2}\right], \tag{12}$$

where $e = \sqrt{(a+2\lambda_2)/b}$ and $f = 1/[2(a+2\lambda_2)]$. The first root represents the separation between the nonoscillating regime IV and the multifrequency region II. The positive of the two conjugate roots defines the boundary between the supercritical regime I and the two in-phase regime I′. Since the coupling constant cannot be imaginary, we obtain a lower bound for the fitting parameter $k_1$, which is given by

$$k_1 \geqslant \frac{2[(\lambda_2 e - F_0)(1 + \lambda_2 f)]^{1/3}}{(\lambda_2 f - 1)^{2/3}\omega^{2/3}} \equiv 2\beta. \tag{13}$$

Next there is a curve that separates the entrainment region III from the subcritical region II. The analytical expression

$$c_{xy} = \frac{4a^3}{27(a + 2\lambda_1)} + \lambda_2\sqrt{\frac{4a}{3b}} \tag{14}$$

was found by transforming the governing equations for the $X_2$ array into polar coordinates and then applying the techniques similar to our earlier work [6]. The analytically obtained boundary curves, with $k_1 = 3.8\beta$, are shown (dashed curves) in Fig. 5.

## VI. CONCLUDING REMARKS

We have used a model-independent approach that emphasizes the symmetries of a network of coupled Duffing elements to demonstrate the idea that certain frequency down-conversion patterns can be induced by the network topology—i.e., the number of elements and type of coupling. The proposed coupling schemes extend to larger networks where even lower-frequency down-conversion ratios can be achieved. The frequency down-conversion described here may have many applications in communication and signal processing where converting a high-frequency signal down to a lower frequency is desirable to avoid the limitations (mainly speed) of ADCs, for example. The down-conversion effect is direct, very fast, efficient, and avoids a noise floor that could be introduced by the generator of the heterodyne signal. By suitably adjusting the array and coupling topologies, the down-conversion ratio in any given application can be readily adjusted to $1/m$ ($m$ integer). Experiments, carried out on a network of coupled overdamped Duffing elements (the underpinnings of an electric field sensor [6]) have validated all the results of this paper; the experimental results will be presented in an upcoming (longer) article.

## ACKNOWLEDGMENTS

We acknowledge support from the Office of Naval Research (Code 30) and SPAWAR internal (S&T) program. A.P. was also supported in part by National Science Foundation Grants No. CMS-0625427 and No. CMS-0638814.

[1] A. Takamatsu, R. Tanaka, H. Yamada, T. Nakagaki, T. Fujii, and I. Endo, Phys. Rev. Lett. **87**, 078102 (2001); A. Takamatsu, T. Fujii, and I. Endo, *ibid.* **85**, 2026 (2000); Y. Loewenstein, Y. Yarom, and H. Sompolinsky, Proc. Natl. Acad. Sci. U.S.A. **98**, 8095 (2002); Y. Loewenstein and H. Sompolinsky, Phys. Rev. E **65**, 051926 (2002).

[2] J. D. Crawford and E. Knobloch, Annu. Rev. Fluid Mech. **23**, 341 (1991).

[3] M. Golubitsky and I Stewart, in *Geometry, Dynamics, and Mechanics: 60th Birthday Volume for J. E. Marsden*, edited by P. Holmes, P. Newton, and A. Weinstein (Springer-Verlag, Berlin, 2002), pp. 243–286; M. Golubitsky, M. Nicol, and I. Stewart, J. Nonlinear Sci. **14**, 207 (2004); D. Armbruster and P. Chossat, Phys. Lett. A **254**, 269 (1999); M. Golubitsky and I. N. Stewart (unpublished).

[4] V. In, A. Kho, J. Neff, A. Palacios, P. Longhini, and B. Meadows, Phys. Rev. Lett. **91**, 244101 (2003).

[5] A. Bulsara, V. In, A. Kho, P. Longhini, A. Palacios, W. J. Rappel, J. Acebron, S. Baglio, and B. Ando, Phys. Rev. E **70**, 036103 (2004).

[6] V. In, A. Palacios, A. Bulsara, P. Longhini, A. Kho, J. D. Neff, S. Baglio, and B. Ando, Phys. Rev. E **73**, 066121 (2006).

[7] A. Palacios, R. Carretero-Gonzalez, P. Longhini, N. Renz, V. In, A. Kho, J. D. Neff, B. K. Meadows, and A. R. Bulsara, Phys. Rev. E **72**, 026211 (2005).

[8] B. Dionne, M. Golubitsky, and I. Stewart, Nonlinearity **9**, 559 (1996); **9**, 575 (1996).

[9] V. In, A. R. Bulsara, A. Palacios, P. Longhini, and A. Kho, Phys. Rev. E **72**, 045104(R) (2005).

[10] E. Doedel and X. Wang, Computer code AUTO94 software for continuation and bifurcation problems in ordinary differential equations, California Institute of Technology (1994).

[11] P. Ashwin, G. P. King, and J. W. Swift, Nonlinearity **3**, 585 (1990).